Theoretical Studies of N_2O Adsorption and Reactivity to N_2 and NO on Rh(111)

Jean-François Paul,[†] Javier Pérez-Ramírez,[‡] Francisco Ample,[§] and Josep M. Ricart*[,§]

Laboratoire de Catalyse de Lille, USTL/CNRS, F-59655 Villeneuve d'Ascq Cedex, France, Catalysis and Nitric Acid Technology, Yara Technology Centre Porsgrunn, P.O. Box 2560, N-3908 Porsgrunn, Norway, and Departament de Química Física i Inorgànica, Universitat Rovira i Virgili, E-43005 Tarragona, Spain

Received: April 29, 2004; In Final Form: July 13, 2004

Periodic DFT calculations have been performed to investigate the adsorption, activation, and reactivity of N_2O on a Rh(111) surface. Several adsorption modes in a narrow range of energies have been found. The most stable situation corresponds to a weak bonding (0.39 eV) via the N-terminal atom on top of a Rh atom, with the lineal N_2O molecule situated nearly perpendicular to the surface. Other flat adsorption modes via the two N atoms or the terminal N and O atoms have also been identified, with adsorption energies around 0.20 eV. These modes activate the molecule by weakening the N−O or N−N bonds, leading to its dissociation and subsequent formation of N_2 or NO. Mechanisms leading to these products have been analyzed, identifying the intermediates and transition states. Both pathways were found to be exothermic but decomposition to N_2 presents significantly lower activation barriers and higher kinetic constants.

1. Introduction

Nitrous oxide (N_2O) is a harmful gas in our environment, contributing to the ozone layer depletion and to the greenhouse effect (310 and 21 times more powerful than CO_2 and CH_4, respectively).[1] The N_2O emission associated with chemical production (namely, in nitric acid manufacture) and stationary combustion processes is concentrated in a limited number of large sources and can be reduced in the short term. Catalytic decomposition of N_2O into N_2 and O_2 represents an attractive and cost-effective technology to reduce N_2O emissions in tail gases.[2,3] Rh-based catalysts on different supports, including single oxides, zeolites, and mixed oxides derived from hydrotalcites, are considered as the most active systems for direct N_2O decomposition at low temperature (<550 K), as compared to catalysts based on other noble metals (Ru, Pd, Pt) and transition metals (Cu, Co, Fe).[4−11]

Classically, the reaction over oxide catalysts is described by the kinetic scheme in eqs 1−4.[12] The reaction is initiated by the adsorption of the N_2O molecule at the active center (eq 1), followed by its decomposition, giving formation of N_2 and a surface oxygen (eq 2). This surface oxygen can desorb by direct reaction with another N_2O (eq 3, Eley−Rideal type) or by recombination of adsorbed oxygen atoms (eq 4, Langmuir−Hinshelwood type). The steps of N_2O adsorption and oxygen recombination are generally assumed to be in quasi-equilibrium under the reaction conditions. In practice, eqs 1 and 2 are combined to give eq 5, since not all the adsorption sites in the catalyst are active for the decomposition.[13] Application of a tracer technique, pulsing $N_2{}^{16}O$ over $^{18}O_2$-pretreated Rh black and Rh/USY catalysts at 493 K, indicated that O_2 desorption occurs via recombination of atomic oxygen species (eq 3),[14,15] while isotopic transient studies of N_2O decomposition over Pt−Rh alloy gauze at 1023 K have identified two separate routes of oxygen formation represented by eqs 3 and 4.[16]

$$N_2O + * \leftrightarrow N_2O* \quad (1)$$

$$N_2O* \rightarrow N_2 + O* \quad (2)$$

$$N_2O + O* \rightarrow N_2 + O_2 + * \quad (3)$$

$$2O* \leftrightarrow O_2 + 2* \quad (4)$$

$$N_2O + * \rightarrow N_2 + O* \quad (5)$$

$$N_2O + * \rightarrow NO + N* \quad (6)$$

Experimental studies have been published on the adsorption and decomposition of N_2O on well-defined metallic surfaces.[17−32] Li and Bowker[17] applied molecular beam adsorption and reaction in combination with LEED and XPS and concluded that N_2O decomposes to N_2 at low temperature on Rh(111) and Rh(110). In a related isothermal kinetic study using molecular beams, Zaera and Gopinath[18,19] postulated that N_2O may be an intermediate species during the NO reduction to N_2 by CO over Rh(111). On this basis, a competitive decomposition of adsorbed N_2O into N_2 or NO, according to eqs 5 and 6, can be in principle envisaged, although the formation of NO upon interaction of N_2O with catalyst surfaces in steady-state or transient experiments has not been reported in the literature, N_2 and O_2 being the decomposition products. Despite extensive work, the mechanism of NO reduction to N_2 by CO over Rh-based catalysts has not been definitively elucidated, and the particular implication of N_2O as a reaction intermediate in this process is controversial.[33] Further understanding requires the determination of the most stable adsorption mode and reactivity of the N_2O molecule on close-packed metallic surfaces.

Theoretical studies of N_2O adsorption on metal surfaces are scarce. To our knowledge, only the adsorptions of N_2O on Pd(110),[30,34,35] Ni(755),[36] and Pt(111)[37] have been investigated. N_2O adsorbs on Pd(110) via both terminal N and O atoms,

* To whom correspondence should be addressed Fax: +34 977 559 563. E-mail: ricart@quimica.urv.es.
[†] USTL/CNRS.
[‡] Yara Technology Centre Porsgrunn.
[§] Universitat Rovira i Virgili.

10.1021/jp048138h CCC: $27.50
Published on Web 10/12/2004

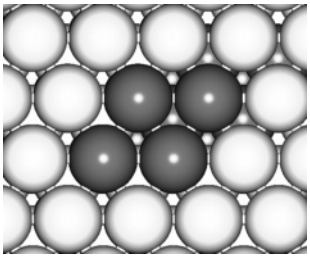

Figure 1. Rh(111) surface (2 × 2) supercell used in this study.

although the energetic differences between the various adsorption modes are very small and the adsorption energies depend on the coverage of the surface. On Ni(755) or Ni[6(111)×(100)], various adsorption modes have been considered.[36] The adsorption energies on the flat (111) surface were small, independent of the geometry analyzed. Oppositely, adsorption energies around 1 eV have been computed for the adsorption on steps, the molecule being adsorbed via terminal N and O atoms. Orita and Itoh[36] stressed that the activation energy for N_2O decomposition on step sites is very small, as some geometry optimizations lead to formation of N_2 and O. Theoretical studies on N_2O decomposition have been carried out on different systems, including atomic 3d transition metals and metal zeolites[38−40] Both experimental[41,42] and theoretical[38,43,44] N_2O decomposition studies have been carried out over metal oxides. However, on an oxide surface, the most important parameter is the polarization of the molecule induced by the electrostatic field, and hence, the mechanisms are in principle not extrapolable to metals.

On the basis of the above analysis, this work was undertaken to obtain a rational understanding of the adsorption, activation, and reactivity of N_2O over rhodium. These are essential aspects in catalyst design for an optimized performance. To this end, periodic DFT calculations on N_2O adsorption on a Rh(111) surface have been carried out. A large number of adsorption geometries by one or two atoms on the various classical adsorption sites have been systematically computed, and likely reaction pathways for the N_2O decomposition into N_2 or NO have been analyzed.

2. Computational Details

The ab initio calculations were performed with the Vienna Ab-initio Simulation Program (VASP).[45,46] It is based on Mermin's finite-temperature local density functional theory (DFT)[47] and solves the Kohn−Sham equations with the development of the one-electron wave function in a basis of plane waves. The electron−ion interactions are described through the projector augmented wave (PAW) method.[48,49] The resolution of the Kohn−Sham equations is performed using an efficient matrix diagonalization routine based on a sequential band-by-band residual minimization method for the one-electron energies. An improved Pulay mixing is used to update the charge density. The optimization of the atomic positions is performed via a conjugate gradient minimization of the total energy using the Hellmann−Feyman forces on the atoms.

In this study, a 2 × 2 super cell (Figure 1) containing four Rh atoms per layer and five layers in the *z* direction was used. A vacuum of 10 Å has been added to separate the layers. The three upper rows were allowed to relax, while the two lower ones were kept fixed at the bulk geometry to simulate bulk constraints. The calculations were performed with at least five *k*-points (separation below 0.05 $Å^{-1}$), a cutoff energy of 400 eV, and a Methfessel−Paxton smearing[50] with $\sigma = 0.1$ eV. Preliminary calculations were performed to optimally adjust the previous parameters. The exchange-correlation function originally developed by Ceperley and Alder and parametrized by Perdew and Zunger[51] was used, accounting for the generalized gradient corrections proposed by Perdew et al.[52]

The Rh−Rh distance was the one corresponding to the optimized bulk, with a lattice parameter of 3.85 Å, very close to the experimentally determined value of 3.803 Å. The geometry optimization includes all degrees of freedom of the adsorbates and the two uppermost metal layers, while the three lowest metal planes were kept fixed at the bulk geometry. The adsorption energy (E_{ads}) was calculated according to

$$E_{ads} = E_{sub} + E_{N_2O} - E_{N_2O/sub}$$

where E_{sub} is the naked substrate energy, E_{N_2O} is the energy of the molecule in the gas phase, and $E_{N_2O/sub}$ is the energy of the adsorbed molecule. A positive E_{ads} indicates an exothermic process.

To localize the various transition states (TSs), we have used the nudge elastic band (NEB)[53] method implemented in VASP, modified following the Johnson group method,[54] to have a significant image density close to that of the transition state. To characterize the TSs, frequency calculations have been performed through numerical differentiation of the force matrix including all the optimized degrees of freedom, i.e., the coordinates of the molecule and of the atoms of the three upper rows of the slab. It has thus been checked that all the TSs presented in this study have one, and only one, imaginary frequency. Using the computed frequencies for the normal modes, the zero-point energy (ZPE) correction has been included for the most stable structures. The pressure diagrams have been determined by application of a simple thermodynamic model[55−58] where the gas phase plays the role of a reservoir in equilibrium with the substrate and the adsorbed phase. Then, the gas phase imposes its pressure and temperature on the adsorbed phase. Only the chemical potential of the gas-phase reference is explicitly considered, while the effects of the pressure and temperature on the metal have been neglected.

The projected density of states (PDOS) has been calculated using a 7 × 7 × 1 *k*-point grid by projecting the wave function onto the s, p, or d spherical harmonics, within the limit of a sphere centered on the atom in consideration.

3. Results and Discussion

3.1. Adsorption of N_2O on Rh(111). The N_2O molecule in the gas phase is linear, with $C_{\infty v}$ symmetry and a $^1\Sigma^+$ electronic configuration. The calculated N−N and N−O distances, 1.153 and 1.209 Å, respectively, are in good agreement with the experimentally determined values (1.1273 and 1.1851 Å)[59] and other theoretical calculations using a variety of methods.[60−62]

As reported by Kokalj et al.,[30,34,35] several adsorption modes are possible on a metal surface. These authors computed that the adsorption energies for N_2O adsorption on Pd(110) by the two terminal atoms (N_t, O_t) and by the N_t atom are equivalent (0.36 and 0.40 eV, respectively). It is thus important to carry out a systematic study of the N_2O adsorption on the surface considered in our study, Rh(111). To this end, five different adsorption modes were computed, including the two $\eta 1$ modes (by N_t or O_t) and the three $\eta 2$ modes ((N_t, N_c), (N_t, O_t), and (N_c, O_t)). In some cases, the displacement of the adsorbed N_2O molecule on the Rh surface between the high-symmetry points (top, bridge, hollow fcc, and hollow hcp) has been investigated. The adsorption energies as well as other relevant geometrical parameters are summarized in Table 1, including the ZPE

TABLE 1: Adsorption Energy of N_2O on Rh(111) and Derived Geometrical Parameters[a]

					bond distance/Å		
hapticity	bonded atoms	position[b]	figure	E_{ads}/eV	N−N	N−O	Rh−(N or O)
gas phase					1.14	1.21	
$\eta1$	N_t	T	2a	0.39 (0.39)	1.15	1.21	1.98
		B		0.05	1.16	1.21	2.18
		H		0.00	1.17	1.21	2.25
	O	T		−0.03	1.15	1.20	2.95
		B		0.03	1.15	1.20	3.05
		H		−0.05	1.15	1.20	2.95
$\eta2$	N_t−N_c	B−T	2b	0.31 (0.35)	1.35	1.22	2.05/2.01
		T−T(di-σ)	2c	0.19 (0.17)	1.25	1.24	2.00/2.08
		T−T(π)	2d	−0.29	1.19	1.22	2.18/2.20
	N_t−O	T−T(di-σ)	3a	0.30 (0.31)	1.20	1.32	2.00/2.09
		B−T	3b	0.17 (0.21)	1.26	1.30	2.12/2.08
	N_c−O	T−T(di-σ)		−0.28	1.17	1.37	2.07/2.07
		T−T(π)	4	−0.15	1.15	1.20	2.95/2.71

[a] The E_{ads} values in parentheses include the ZPE correction. [b] T = top, B = bridge, and H = hollow (both fcc and hcp positions have been analyzed).

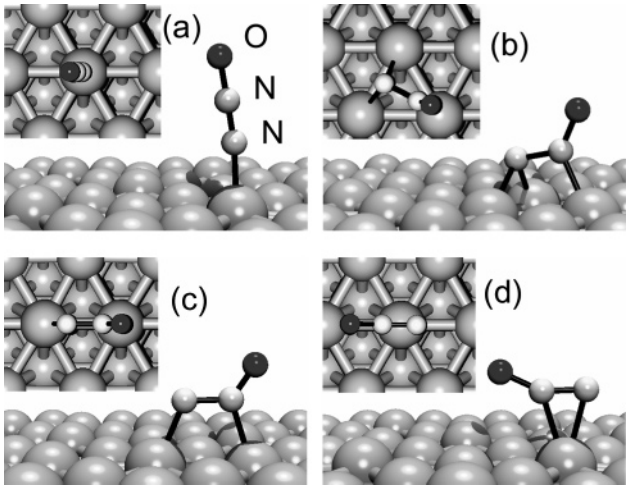

Figure 2. Different adsorption modes of N_2O on Rh(111): (a) N $\eta1$ top adsorption, (b) N $\eta2$ adsorption bridge−top, (c) N $\eta2$ adsorption top−top, and (d) π adsorption. Periodicity has been omitted for clarity.

correction for the most stable structures. No stable adsorption mode involving the three atoms of the molecule was identified.

3.1.1. Adsorption Modes $\eta1$. The most stable adsorption mode is the adsorption through the terminal N_t atom on top of one Rh atom (Figure 2a), yielding an adsorption energy of E_{ads} = 0.39 eV. This is in agreement with the general behavior found for other widely studied adsorbates such as CO or NO in the sense that the preferred adsorption mode is expected to be via the atom with the lowest electronic density, since this leads to a decreased Pauli repulsion between the metal surface and the adsorbate. Additionally, the 6σ orbital of N_2O, which is dominated by O, is too low in energy to interact with the metal (see below). The molecule is slightly tilted (about 7°), but as reported by Kobal et al.,[29] the potential energy surface is very flat as a function of the tilting angle. The adsorbed N_2O molecule hardly suffers any distortion (d_{N-N} = 1.145 Å and d_{N-O} = 1.21 Å), even if the Rh−N distance is rather short (d_{Rh-N} = 1.98 Å). The adsorption can be considered as a strong physical adsorption or a weak chemisorption. Accordingly, it is reasonable to suppose that this adsorption mode will preferentially lead to N_2O desorption rather than a chemical dissociation according to eqs 4 and 5. The adsorption by the N_t atom in other positions of the surface is athermic (-0.05 eV < E_{ads} < +0.05 eV), which indicates that the displacement of the adsorbed N_2O molecule on the surface will spontaneously lead to its desorption. The adsorption by the terminal oxygen atom is unstable with a distance between the molecule and the surface greater than 3 Å. Such a configuration corresponds to a physically adsorbed state.

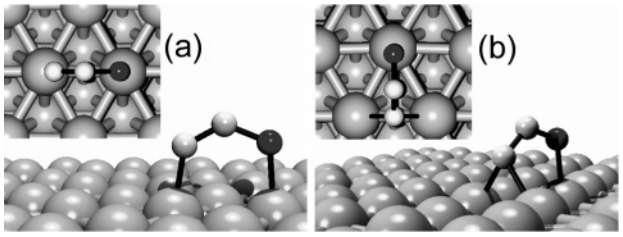

Figure 3. Different adsorption modes of N_2O on Rh(111) via the two terminal atoms: (a) top−top, (b) N in a bridge position and O in a top position.

3.1.2. Adsorption Modes $\eta2$. Among the three types of $\eta2$ adsorption modes, two are stable. The first one is an adsorption via the two N atoms. The adsorption energy is 0.35 eV when the N_t atom is in a bridging position and the N_c atom is in a top position (Figure 2b) and is decreased to 0.17 eV when the N_t atom is also placed in a top position (Figure 2c). This flat adsorption mode is only slightly less stable than the $\eta1$ N_t top adsorption mode described above. The two flat adsorption geometries described are similar to that of the di-σ adsorption mode of the olefins and induce important variation of the molecular geometry.[63,64] Due to the formation of a bond between N_t, N_c, and Rh, the molecule is not linear any longer. The N−N−O angles of the optimized structures in parts b and c of Figure 2 are 123° and 130°, respectively. The variation of the hybridization of the N_c atom leads to an important variation of the N−N distance (1.35 Å for Figure 2b and 1.25 Å for Figure 2c) as compared to that in gas-phase N_2O (1.15 Å). On the contrary, the N−O distance remains very similar. For the N_t-(bridge)−N_c(top) adsorption mode (Figure 2b), the N−N bond is enlarged by 0.20 Å. Hence, as the N−N bond is largely activated while the N−O one is not distorted, this adsorption mode is considered as a suitable starting point for the dissociation of the N_2O molecule according to eq 6, leading to NO and N species adsorbed on the surface.

The adsorption energy can be rationalized in terms of a cost−benefit analysis. The energetic cost to distort the N_2O molecule from the gas phase to that of the adsorbed geometry in parts b and c of Figure 2 is 3.03 and 1.77 eV, respectively. The interaction energy of the previously distorted molecule becomes 3.34 eV for the formation of three Rh−N bonds, since N_t is in a bridging position and N_c is in a top position, and 1.98 eV for the formation of two Rh−N bonds. Thus, the relatively low adsorption energies computed for the adsorption by the two N atoms reflect not merely a weak interaction between the molecule and the surface, but rather the high energy required to deform the N_2O molecule. The last adsorption by the two nitrogen atoms that we have considered is the π mode on top of one Rh atom (Figure 2d). The adsorption energy for this mode is negative (E_{ads} = −0.30 eV), and its deformation energy is less important than those for the previous adsorption modes (E_{def} = 0.55 eV), but the interaction with only one Rh atom is energetically insufficient to stabilize the system.

The adsorption of N_2O on Rh(111) via the two terminal atoms (N_t and O_t) is also stable. An adsorption energy of 0.27 eV is computed when the two terminal atoms are in top positions (Figure 3a). If the nitrogen atom is displaced from a top to a bridge position (Figure 3b), the adsorption energy is reduced

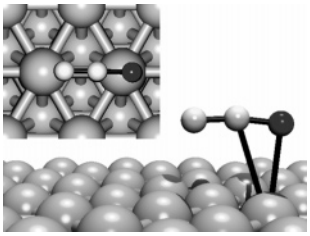

Figure 4. π adsorption of N_2O via the N−O bond.

to 0.21 eV. Once again, the geometries of the adsorbed molecule are very different from the geometry in the gas phase, and N−N−O angles of 128° and 122° are obtained for the configurations represented in parts a and b, respectively, of Figure 3. The associated N−O (1.32 and 1.30 Å) and N−N (1.20 and 1.25 Å) distances are significantly larger compared to those in gas-phase N_2O. The values of the distortion energy are 1.95 and 2.51 eV, which are similar to the computed values in the case of adsorption via the two nitrogen atoms.

The final type of $\eta 2$ adsorption involves the adsorption of N_2O via the central nitrogen and the oxygen atoms (N_c−O). For this case, negative adsorption energies were computed, no matter what starting geometry was applied, thus indicating unstable adsorption. The least unstable adsorption mode corresponds to the top adsorption of both N_c and O in top positions (Figure 4), with $E_{ads} = -0.15$ eV.

To analyze surface coverage effects, it will be necessary to take into account the competition between the vertical adsorption and the two flat modes. However, an increase of the N_2O partial pressure will favor the top adsorption, which involves only one surface Rh atom. To confirm this hypothesis, we have performed calculations at different coverages and computed the effect of the gas-phase pressure on the N_2O surface coverage. The coverage effect on the chemisorption energy is negligible for the top, N_t(top)−N_c(top), and O_t(top)−N_t(top) adsorption modes when a larger 3×3 unit cell is considered, corresponding to a coverage of 0.11, the difference in computed energies being lower than 0.02 eV. The variation for the N_t(bridge)−N_c(top) adsorption mode is slightly larger (0.36 eV vs 0.31 eV for the 2×2 cell). This effect was expected since this adsorption mode involves three Rh atoms. On the 3×3 cell the adsorption energies of the top and N_t(bridge)−N_c(top) modes are similar, but the last one involves an important distortion of the molecule and will correspond to an activated adsorption. The kinetic effect will favor the top adsorption mode. For the $\eta 1$ top mode we have also calculated the effect of the gas-phase pressure on the N_2O surface coverage. Coverages of 0.11, 0.25, 0.33, and 0.5 have been investigated using different units cells. Up to 0.33, corresponding to a $\sqrt{3} \times \sqrt{3}$ unit cell, the binding energies are very similar, close to 0.39 eV. However, for a coverage of 0.5 (2×1 unit cell), the adsorption energy is only 0.03 eV, thus indicating that this is an upper limit for the coverage. The Gibbs free energy for the adsorption reaction $Rh(s) + N_2O(g) \leftrightarrow \theta N_2O$ (adsorbed), where θ stands for the coverage, has been computed using[55−58]

$$\Delta G = \Delta\mu^\circ(T) + RT \ln(P_{N_2O}/P^0)$$

In this expression, it is assumed that the chemical potential difference between the clean and adsorbed surface, $\Delta\mu^\circ$, can be approximated by the electronic energy variation and the chemical potential of the gas-phase molecule is estimated by calculating its partition function. Figure 5 shows the dependence of ΔG on the relative pressure at 298 K for coverages ranging

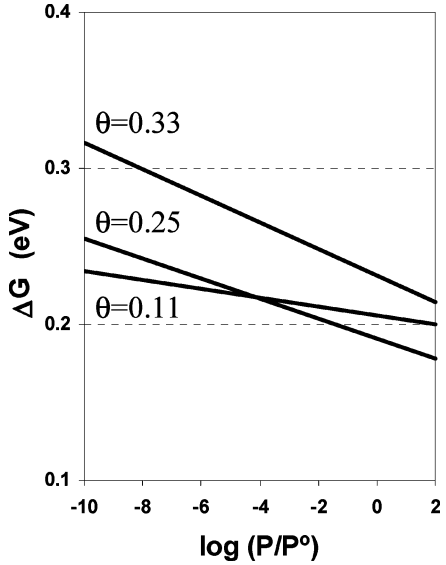

Figure 5. Variation of the Gibbs free energy for the adsorption of N_2O as a function of the decimal logarithm of the relative N_2O pressure for different coverages (θ) at $T = 298$ K.

from 0.33 to 0.11. The N_2O adsorption process is not favored on the Rh(111) surface at 298 K. At this temperature, the coverage will remain low whatever the pressure; for a N_2O partial pressure lower than ca. 10^{-4} bar, the coverage will be 1/9, and it will increase to 1/4 for a higher partial pressure. However, at lower temperatures the adsorption will be spontaneous; for example, $\Delta G^\circ = -0.19$ eV at 100 K. All these data should be cautiously analyzed since the differences in binding energies at low coverage (~0.03 eV) are on the order of the computational accuracy.

Further insights into the bonding mechanism and electronic properties can be obtained using the PDOS of the different systems and a simple frontier orbital model.[65] Figure 6 shows the PDOS for noninteracting free N_2O and the Rh slab, the N_2O adsorbed on top, the most stable mode involving N_t and O, and the $\eta 2$ mode involving the two N atoms.

For N_2O adsorbed on top, the 7σ and 2π orbitals are shifted down in energy (3 and 1.5 eV, respectively), and there appears to be only a small contribution of the metal states at the corresponding energies, but overall, the changes are small, thus suggesting a rather low covalent interaction consistent with a small binding energy. A careful analysis of the projected DOS on the atoms (not shown in the figures) indicates that the atom that participates more in the 7σ orbital of free N_2O is N_t; thus, for the top adsorption this is the more affected orbital. Additionally, the 3π orbital remains nearly unaffected, indicating the absence of back-donation. As the 7σ orbital is of nonbonding nature, the overall interaction does not change the N−N and N−O bonds with respect to those of the free molecule, in agreement with the experimental results of Haq and Hodgson[27] for N_2O adsorption on Pd(110). On the contrary, for the $\eta 2$ modes, the downshift of the 7σ orbital is less important, and the 1π orbitals are upshifted, interchanging the energy order with the 7σ orbital. Moreover, the 2π and 3π orbitals become wider and mix together (in fact, the distortion of the molecule disables a strict classification between σ and π systems), thus indicating an interaction of the π system with the surface. As the 3π orbital is antibonding, its population weakens the intramolecular bonds, thus explaining the longer N−N and N−O bonds. These trends are in qualitative agreement with those

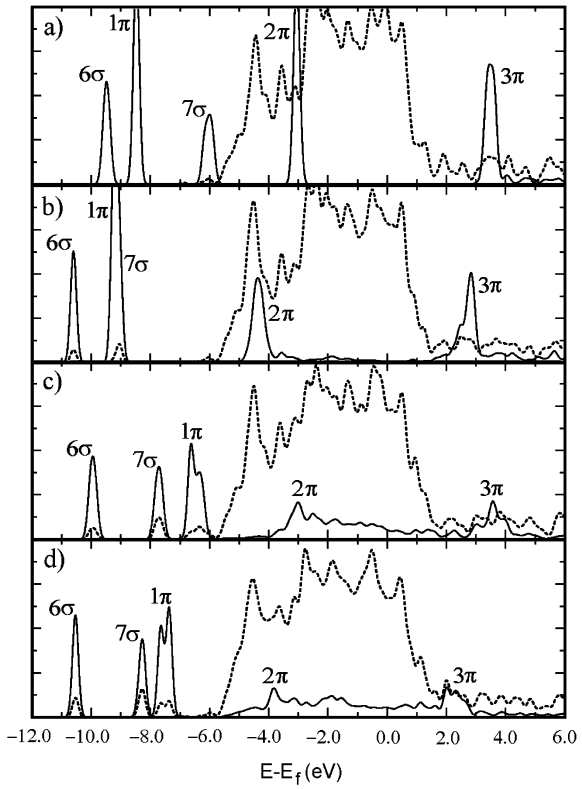

Figure 6. Projected density of states for (a) noninteracting gas-phase N_2O and a Rh slab, (b) adsorbed N_2O on top (Figure 2a), (c) N_t(top)−O(top) (Figure 2c), and (d) N_t(bridge)−N_c(top) (Figure 2b). Key: continuous line, N_2O contribution; dashed line, Rh slab contribution. The labels of the peaks correspond to the molecular states of the gas-phase N_2O.

reported by Kokalj et al.[34] on Pd(110), indicating the similar behavior of both surfaces.

3.2. Reactivity of Adsorbed N_2O on Rh(111). The exhaustive analysis of N_2O adsorption geometries in section 3.1 clearly indicates that Rh(111) can activate both the N−N and the N−O bonds of the N_2O molecule when flat adsorption modes are considered. To determine the most favorable decomposition pathway of N_2O once adsorbed, the activation energies have been computed using the stable adsorption geometries as starting points. We have shown that the most stable adsorption mode is the top adsorption by the terminal nitrogen atom ($E_{ads} = 0.39$ eV). This adsorption mode induces no change in the bond lengths of N_2O (see Table 1) and would likely lead to its desorption rather than further decomposition. Accordingly, the first step for N_2O decomposition should be initiated by the transformation of a top adsorption (Figure 2a) into flat adsorption modes (Figures 2c and 3a).

3.2.1. Mechanism of N_2 Formation. The main decomposition pathway for the N_2O molecule is the formation of N_2 and adsorbed atomic oxygen (eq 5). Since the most stable adsorption mode of N_2 on Rh(111) is in a top position, with an estimated adsorption energy of 0.50 eV,[66] it can be tentatively put forward that the precursor state for such a reaction pathway is represented by Figure 3a. This adsorption mode induces the activation of the N−O bond and increases the N−N distance of the N_2O molecule. Contrarily, the other stable adsorption modes obtained do not increase the N−O bond distance. This would support the surface parallel form of adsorbed N_2O invoked by Liu et al.[32] as a precursor for the N_2 desorption on Rh(110). The geometry of the transition state that leads to this precursor is represented in Figure 7a and involves an activation energy of 0.34 eV.

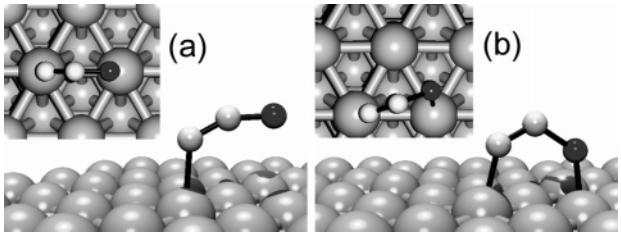

Figure 7. Transition states for (a) the top-[N_tO_t] transformation ($E_{act} = 0.34$ eV) and (b) the N−N−O dissociation ($E_{act} = 0.11$ eV) corresponding to the step leading to N_2 formation.

TABLE 2: Geometrical Parameters of the Transition States

transition state[a]	bond distance/Å				N−N−O angle/deg
	N−N	N−O	Rh−N	Rh−(O or N)	
7a	1.16	1.22	2.14		154
7b	1.19	1.45	1.99	2.03	121
8a	1.18	1.21	2.01	2.71	154
8b	1.28	1.24	2.06	1.98	130
8c	1.86	1.19	1.94	1.93	120

[a] The number given refers to the figure number.

The N−O distance is 1.53 Å, while the N−N distance is 1.19 Å (Table 2), similar to that of gas-phase N_2. This is followed by the dissociation of N_2O into N_2 and atomic O, which are adsorbed in top and hollow positions, respectively. The activation energy of this step is 0.11 eV. The corresponding transition state is represented in Figure 7b. This second step of dissociation, starting for the most stable adsorption mode, is slightly activated and very exothermic ($\Delta E = -1.89$ eV). Starting from the flat adsorption mode, two reaction pathways are eventually possible: (i) decomposition or (ii) conversion to the top adsorption mode. The smaller activation energy for the dissociation (0.11 eV) as compared to the change in adsorption mode (0.27 eV) clearly indicates that the dominant process upon N_2O adsorption on a flat geometry is the decomposition.

3.2.2. Mechanism of NO Formation. The N_2O decomposition into NO and adsorbed atomic nitrogen according to eq 6 can be postulated as a mechanism occurring via three elementary steps. The first step involves the isomerization from the most stable adsorption mode of N_2O to the di-σ adsorption mode via two nitrogen atoms (Figure 2c). This step is endothermic ($\Delta E = 0.22$ eV) with a computed activation energy of 0.36 eV. The transition state is displayed in Figure 8a. The above isomerization is followed by the displacement of the N_t atom from a top to a bridge position. This exothermic step ($\Delta E = -0.18$ eV) is very fast and hardly involves any activation (0.02 eV) (Figure 8b).

Therefore, the displacement of the N_2O molecule on the surface takes place in two steps. The final step is the breaking of the already activated N−N bond, which is a very exothermic step ($\Delta E = -0.81$ eV) with a computed activation energy of 0.41 eV, the transition state being displayed in Figure 8c. An alternative reaction pathway has been investigated, consisting of a displacement of the vertical molecule from a top to a bridge position and then a bending of the molecule to form the bond between the surface and the N_c atom. This scheme has been discarded since the first displacement of the N_t atom in a bridge position would induce the immediate desorption of the N_2O molecule.

The overall reaction path for N_2O adsorption and decomposition on Rh(111) is summarized in Figure 9. The calculations indicate that the decomposition of N_2O to adsorbed N_2 and O

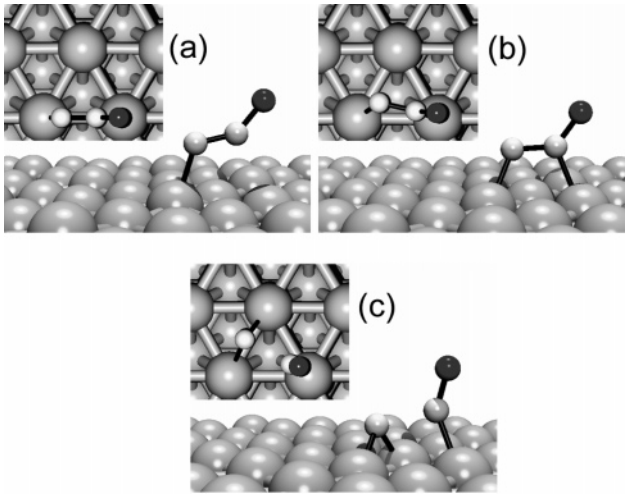

Figure 8. Transition states for (a) the top-[N_tN_t] transformation (E_{act} = 0.36 eV), (b) the displacement on the surface (E_{act} = 0.02 eV), and (c) the NO + N decomposition (E_{act} = 0.41 eV) corresponding to the step leading to NO formation.

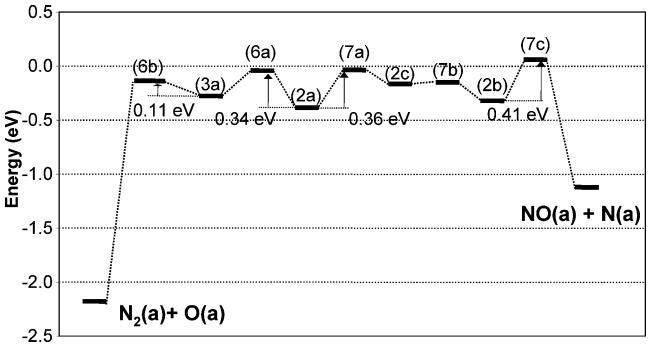

Figure 9. Reaction paths for N_2O activation and decomposition into adsorbed N_2 + O and NO + N. The related figure numbers are given in parentheses. The zero energy level corresponds to a noninteracting surface and N_2O in the gas phase. The energies include the ZPE correction.

species on Rh(111) is an exothermic process. Since the adsorption energy of N_2 on the surface is very low, it rapidly desorbs once produced and leads to a high oxygen coverage on the surface, in agreement with experimental observations. The formation of NO is also an exothermic process, but less exothermic than the formation of N_2. Additionally, starting from the most stable adsorption mode, two transition states of about 0.4 eV must be overcome; thus, it is clear that the favored decomposition process, both thermodynamically and kinetically, is the formation of N_2 and not of NO. Summarizing, the absence of NO during N_2O decomposition over Rh and generally over any catalyst surface is caused principally by a smaller activation energy for N_2 formation than for NO formation, and the small adsorption energy of N_2 molecules on Rh(111). In fact, the adsorption energy is smaller than the activation for N_2O formation, and therefore, N_2 formation can be considered as an irreversible process on Rh(111). Oppositely, the NO adsorption energy of NO (>2.0 eV)[67] is higher than the activation energy for N_2O formation (E_{act} = 1.21 eV). These interrelated processes lead to a preferential N_2 formation upon interaction of N_2O over Rh(111). The kinetic rate constants of the elementary reactions have been estimated within the harmonic transition-state theory.[68,69] The values at 300 and 600 K are shown in Table 3.

The set of elementary steps shown in Figure 9 may also explain the production of molecular nitrogen at relatively high temperatures in the reduction of NO by CO on Rh(111) via the

TABLE 3: Estimated Rate Constant of the Surface Reactions

elementary reaction[a]	k (s^{-1}) T = 300 K	k (s^{-1}) T = 600 K	elementary reaction[a]	k (s^{-1}) T = 300 K	k (s^{-1}) T = 600 K
2a → 3a	1×10^7	2×10^{10}	2c → 2a	3×10^7	1×10^{10}
3a → N_2 + O	1×10^{12}	4×10^{13}	2c → NO + N	3×10^5	2×10^9
2a → 2c	3×10^6	3×10^9	NO + N → 2c	5×10^{-9}	1×10^2

[a] The numbers refer to the figure number.

formation and subsequent decomposition of a N−NO surface intermediate, as proposed by Zaera and Gopinath.[18,19] Although the present activation barrier for the transformation of NO(a) + N(a) to N_2O(a) on Rh(111) is relatively high (1.21 eV), it is lower than the one predicted theoretically by Burch et al.[37] for the N_2O formation on Pt(111) of 1.78 eV from NO(a) + N(a) also via a Langmuir−Hinshelwood mechanism. Accordingly, they ruled out this mechanism at low temperatures and speculated on the possibility of an alternative method involving a $(NO)_2$ dimer species. However, a recent study[31] of the formation of N_2O and N_2 in a steady-state NO + CO reaction on Pd(110) has shown that the pathway through the intermediate adsorbed N_2O prevails below 600 K. From the present results, the formation of N_2O from NO + N does not occur at low temperatures but should be included in the reaction scheme at higher temperatures. At 600 K, the rate constant for this reaction is estimated to be 10^2 s^{-1} (Table 3).

4. Conclusion

The interaction of N_2O with the Rh(111) surface and its decomposition into N_2 + O or NO + N have been studied using density functional theory calculations with a slab model. From the present calculations, it is concluded that the most stable adsorption mode is via the N-terminal, on top of a Rh atom on the surface, with a binding energy of ∼0.40 eV. There are two more stable structures in a narrow range of energies involving the interaction of the two N atoms or the N-terminal and the O atoms. Thus, the adsorption energies are small, independent of the type of adsorption mode considered. In competition with other molecules such as NO, at high temperatures, the N_2O coverage will be small on the close-packed rhodium surface, inhibiting the decomposition. We have followed two possible reaction paths, starting from flat adsorption modes via the two terminal atoms (N_t and O_t), which results in activation in the sense that the N−N and N−O bonds are elongated with respect to those of the free N_2O molecule. The most stable adsorption mode is via the terminal N atom, which would preferentially lead to N_2O desorption, since the molecule is not activated and the activation energy for desorption is comparable to that involving surface reactions leading to reactive flat adsorption modes. The decomposition of N_2O on the Rh(111) surface is an exothermic process, adsorbed N_2 and O being thermodynamically favorable products. In addition, the comparison of the activation energy of the two decomposition pathways indicates that the main decomposition path will be the formation of N_2 and not the formation of NO, in agreement with experimental results over Rh-based catalysts.

Acknowledgment. Funding from the Spanish Ministerio de Ciencia y Tecnología (Grant BQU2002-04029-CO2-02) and the Catalan Government (Grant 2001SGR00315) is acknowledged. F.A. is indebted to the Universitat Rovira i Virgili for a predoctoral grant. Research was partially supported by the Improving the Human Potential Programme, Access to Research

Infrastructures, under Contract HPRI-1999-CT-00071 established between the European Community and CESCA-CEPBA. Computer time was also provided by the Centre de Resources Informatique of Lille University.

References and Notes

(1) Pérez-Ramírez, J.; Kapteijn, F.; Schöffel, K.; Moulijn, J. A. *Appl. Catal., B: Environ.* **2003**, *44*, 117.
(2) Pérez-Ramírez, J.; Kapteijn, F.; Mul, G.; Xu, X.; Moulijn, J. A. *Catal. Today* **2002**, *76*, 55.
(3) Pérez-Ramírez, J.; Kondratenko, E. V. *Chem. Commun.* **2004**, *4*, 376.
(4) Doi, K.; Wu, Y. Y.; Takeda, R.; Matsunami, A.; Arai, N.; Tagawa, T.; Goto, S. *Appl. Catal., B: Environ.* **2001**, *35*, 43.
(5) Li, Y.; Armor, J. N. *Appl. Catal., B: Environ.* **1992**, *1*, L21.
(6) Dann, T. W.; Schulz, K. H.; Mann, M.; Collings, M. *Appl. Catal., B: Environ.* **1995**, *6*, 1.
(7) Imamura, S.; Kitao, T.; H. Kanai, H.; Shono, H. S.; Utani, K.; Jindai, H. *React. Kinet. Catal. Lett.* **1997**, *61*, 201.
(8) Yuzaki, K.; Yarimizu, T.; Aoyagi, K.; Ito, S.; Kunimori, K. *Catal. Today* **1998**, *45*, 129.
(9) Oi, J.; Obuchi, A.; Bamwenda, G. R.; Ogata, A.; Yagita, H.; Kushiyama, S.; Mizuno, K. *Appl. Catal., B: Environ.* **1997**, *12*, 277.
(10) Pérez-Ramírez, J.; Overeijnder, J.; Kapteijn, F.; Moulijn, J. A. *Appl. Catal., B: Environ.* **1999**, *23*, 59.
(11) Alini, S.; Basile, F.; Bologna, A.; Montanari, T.; Vaccari, A. *Surf. Sci. Catal.* **2002**, *143*, 131.
(12) Kapteijn, F.; Rodríguez-Mirasol, J.; Moulijn, J. A. *Appl. Catal., B: Environ.* **1996**, *9*, 25.
(13) Kobayashi, H.; Kobayashi, M. *Catal. Rev.—Sci. Eng.* **1974**, *10*, 139.
(14) Tanaka, S.; Yuzaki, K.; Ito, S.; Uetsuka, H.; Kameoka, S.; Kunimori, K. *Catal. Today* **2000**, *63*, 413.
(15) Tanaka, S.; Yuzaki, K.; Ito, S.; Kameoka, S.; Kunimori, K. *J. Catal.* **2001**, *200*, 203.
(16) Kondratenko, E. V.; Pérez-Ramírez, J. *Catal. Lett.* **2003**, *91*, 211.
(17) Li, Y.; Bowker, M. *Surf. Sci.* **1996**, *348*, 1−2, 67.
(18) Zaera, F.; Gopinath, C. S. *Chem. Phys. Lett.* **2000**, *332*, 209
(19) Zaera, F.; Gopinath, C. S. *J. Mol. Catal. A.: Chem.* **2001**, *167*, 23.
(20) Avery, N. R. *Surf. Sci.* **1983**, *131*, 501.
(21) Cornish, J. C. L.; Avery, N. R. *Surf. Sci.* **1990**, *235*, 209.
(22) Ceballos, G.; Wende, H.; Baberschke, K.; Arvanitis, D. *Surf. Sci.* **2001**, *15*, 482.
(23) Väterlein, P.; Krause, T.; Bässler, M.; Fink, R.; Umbach, E.; Taborski, J.; Wüstenhagen, V.; Wurth, W. *Phys. Rev. Lett.* **1996**, *76*, 4749.
(24) Hoffman, D. A.; Hudson, J. B. *Surf. Sci.* **1987**, *180*, 77.
(25) Sau, R.; Hudson, J. B. *J. Vac. Sci. Technol.* **1981**, *18*, 607.
(26) Ohno, Y.; Kimura, K.; Bi, M.; Matsushima, T. *J. Chem. Phys. B* **1999**, *110*, 8221.
(27) Haq, S.; Hodgson, A. *Surf. Sci.* **2000**, *463*, 1.
(28) Ohno, Y.; Kobal, I.; Horino, H.; Rzeznicka, I.; Matsushima, T. *Appl. Surf. Sci.* **2001**, *273*, 169.
(29) Kobal, I.; Kimura, K.; Ohno, Y.; Matsushima, T. *Surf. Sci.* **2000**, *445*, 472.
(30) Kokalj, A.; Kobal, I.; Horino, H.; Ohno, Y.; Matsushima, T. *Surf. Sci.* **2002**, *506*, 196.
(31) Ma, Y.; Rzeznika, I.; Matsushima, T. *Chem. Phys. Lett.* **2004**, *388*, 201.
(32) Liu, S.; Horino, H.; Kokalj, A.; Rzeznicka, I.; Imamura, K.; Ma, Y.; Kobal, I.; Ohno, Y.; Hiratsuka, A.; Matsushima, T. *J. Phys. Chem. B* **2004**, *108*, 3828.
(33) Zhdanov, V. P.; Kasemo, B. *Surf. Sci. Rep.* **1997**, *29*, 31.
(34) Kokalj, A.; Kobal, I.; Matsushima, T. *J. Phys. Chem. B* **2003**, *107*, 2741.
(35) Kokalj, A. *Surf. Sci.* **2003**, *213*, 532.
(36) Orita, H.; Itoh, N. *Surf. Sci.* **2004**, *550*, 166.
(37) Burch, R.; Daniells, S. T.; Hu, P. *J. Chem. Phys.* **2002**, *117*, 2902.
(38) Zhang, Y.; Sun, Y.; Cao, A.; Liu, J.; Fan, G. *J. Mol. Struct.: THEOCHEM* **2003**, *623*, 245.
(39) Delabie, A.; Vinckier, C.; Flock, M.; Pierloot, K. *J. Phys. Chem. A* **2001**, *105*, 5479.
(40) Snis, A.; Miettinen, H. *J. Phys. Chem. B* **1998**, *102*, 2555−2561.
(41) Lu, X.; Xu, X.; Wang, N.; Zhang, Q. *J. Phys. Chem. B* **1999**, *103*, 3373.
(42) Yakovlev, A. L.; Zhidomirov, G. M.; Van Santen, R. A. *Catal. Lett.* **2001**, *75*, 45.
(43) Karlsen, E. J.; Pettersson, L. G. M. *J. Phys. Chem. B* **2002**, *106*, 5719.
(44) Karlsen, E. J.; Nygren, M. A.; Pettersson, L. G. M. *J. Phys. Chem. A* **2002**, *106*, 7868.
(45) Kresse, G.; Hafner, J. *J. Phys. Rev. B* **1993**, *47*, C558.
(46) Kresse, G.; Furthmüller, J. *J. Comput. Mater. Sci*. **1996**, *6*, 15.
(47) Mermin, N. D. *Phys. Rev.* **1965**, *137*, 1141.
(48) Vanderbilt, D. *Phys. Rev. B* **1980**, *41*, 7892.
(49) Kresse, G.; Furthmüller, J. *Comput. Mater. Sci.* **1994**, *6*, 8245.
(50) Methfessel, M.; Paxton, A. T. *Phys. Rev. B* **1989**, *40*, 3616.
(51) Perdew, J. P.; Zunger, A. *Phys. Rev. B* **1981**, *23*, 5048.
(52) Perdew, J. P.; Chevary, J. A.; Vosko, S. H.; Jackson, K. A.; Pedersen, M. R.; Singh, D. J.; Frolais, C. *Phys. Rev. B* **1992**, *46*, 6671.
(53) Mills, G.; Jónsson, H. *Phys. Rev. Lett.* **1994**, *72*, 1124.
(54) Henkelman, G.; Uberuaga, B. P.; Jónsson, H. *Chem. Phys.* **2000**, *113*, 9901.
(55) Reuter, K.; Scheffler, M. *Phys. Rev. B* **2002**, *65*, 035406.
(56) Bollinger, M. V.; Jacobsen, K. W.; Nørskov, J. K. *Phys. Rev. B* **2003**, *67*, 085410.
(57) Cristol, S.; Paul, J. F.; Payen, E.; Bougeard, D.; Clémendot, S.; Hutschka, F. *J. Phys. Chem. B* **2000**, *104*, 11220.
(58) Raybaud, P.; Hafner, J.; Kresse, G.; Kasztelan, S.; Toulhoat, H. *J. Catal.* **2000**, *189*, 129.
(59) Teffo, J.-L.; Chendin, A. *J. Mol. Spectrosc.* **1989**, *138*, 134.
(60) Lesar, A.; Hodoseck, M. *J. Chem. Phys.* **1998**, *109*, 9410.
(61) Wang, F.; Harcourt, R. D. *J. Phys. Chem. A* **2000**, *104*, 1304.
(62) Solans-Monfort, X.; Sodupe, M.; Branchadell, V. *Chem. Phys. Lett.* **2003**, *368*, 242.
(63) Anson, C. E.; Sheppard, N.; Bender, B. R.; Norton, J. R. *J. Am. Chem. Soc.* **1999**, *121*, 529
(64) Valcárcel, A.; Ricart, J. M.; Clotet, A.; Markovits, A.; Minot, C.; Illas, F. *Surf. Sci.* **2002**, *519*, 250.
(65) Hoffmann, R. *Angew. Chem., Int. Ed. Engl.* **1987**, *26*, 846.
(66) Ample, F.; Ricart, J. M.; Clotet, A.; Curulla, D.; Niemantsverdriet, J. W. *Chem. Phys. Lett.* **2004**, *385*, 52.
(67) Loffreda, D.; Simon, D.; Sautet, P. *Chem. Phys. Lett.* **1998**, *291*, 15.
(68) Laidler, K. J. *Chemical Kinetics*, 3rd ed.; Harper Collins: New York, 1987.
(69) Loffreda, D.; Simon, D.; P. Sautet, P. *J. Catal.* **2003**, *213*, 211.